JOURNAL OF AIRCRAFT
Vol. 45, No. 6, November–December 2008

Insectlike Flapping Wings in the Hover Part 2: Effect of Wing Geometry

Salman A. Ansari,* Kevin Knowles,† and Rafał Żbikowski‡
Cranfield University, Defence Academy of the United Kingdom, Shrivenham, England SN6 8LA, United Kingdom

DOI: 10.2514/1.35697

The aerodynamic design of a flapping-wing micro air vehicle requires a careful study of the wing design space to ascertain the best combination of parameters. A nonlinear unsteady aerodynamic model developed by the authors is used to make such a study for hovering insectlike flapping wings. The work is characterized, in particular, by the insights it provides into flapping-wing flows and the use of these insights for aerodynamic design. The effects of wing geometry on the aerodynamic performance of such flapping wings are investigated by comparing the influence on a number of synthetic planform shapes while varying only one parameter at a time. Best performance appears to be for wing shapes that have nearly straight leading edges and more area outboard, where flow velocities are higher. Other important trends are also identified and practical considerations are noted. When possible, comparisons are also drawn with quasi-steady expectations and discrepancies are explained.

Nomenclature

AR	=	aspect ratio ($2R^2/S$)
C_L	=	lift coefficient ($\mathcal{L}/\frac{1}{2}\rho V^2 S$)
c	=	chord length, m
$\bar{c}$	=	mean chord length (S/R), m
$\mathcal{D}$	=	drag, N
d	=	wing-offset distance ($l - R$), m
f	=	flapping frequency, Hz
k	=	reduced frequency ($f\bar{c}/2V$)
$\mathcal{L}$	=	lift, N
l	=	(radial) wing extent, m
$\mathcal{Q}$	=	torque, Nm
R	=	wing length, m
S	=	planform area of one wing, m^2
s	=	number of semichords traveled
$\mathcal{T}$	=	thrust, N
V	=	velocity, m/s
x	=	dummy variable
α	=	pitch angle
ρ	=	fluid density, kg/m^3
Φ	=	stroke amplitude
ω	=	sweep rate, rad/s

I. Introduction

MICRO air vehicles (MAVs) are small (approximately 150 mm) handheld flying machines that are attractive for flight inside buildings, caves, and tunnels. Such indoor flight is of significant military and civilian value and leads to the requirement of distinct characteristics that include small size, low flight speed, hovering capability, high maneuverability at low speeds, and small acoustic signature, among other things. As discussed elsewhere [1–4], insectlike flapping is a proven solution meeting the particular requirements for an agile MAV for operation in confined spaces. Little previous work has been published that aims to produce an optimized wing aerodynamic design for such vehicles.

Although insect flapping wings offer a proven solution and are abundant in nature (there are over 170,000 species of flying insects), little is known about the optimality of their wing design. Crucially, the wings are responsible not only for lift but also for propulsion and maneuvers. The work presented in this paper addresses this issue of converging on preferred design characteristics for an insectlike flapping wing in terms of wing geometry. This is the second of a two-part paper; the effects of wing kinematics are considered in part 1 [5].

Ellington's [6] seminal work rejuvenated interest in insect flight, but it is only recently that attention has been directed toward the design of vehicles that use insectlike flapping wings, particularly at the MAV scale [1–3]. In a later study, Ellington [7] proposed design guidelines based on scaling from nature, but this does not give physical insight or allow design optimization. Most other studies have concentrated essentially on the effect of kinematics parameters on the performance of insectlike flapping wing (see, for example, [5,8–16]). The current study appears to be the first of its kind to consider wing geometric parameters. It is part of a wider campaign at Cranfield University (Shrivenham) aimed at the aerodynamic design of insectlike flapping wings for MAVs. After some initial work using simple quasi-steady models [17,18], Ansari et al. [19,20] used a more complex nonlinear unsteady aerodynamic model for insectlike flapping wings in the hover to conduct a more advanced investigation [21]. The current work is a further extension of this study and now considers the effects of a wider range of wing planforms and other wing-design parameters. This work also includes more detailed analysis based on considerations of flow physics in the flapping-wing regime and, in doing so, provides much-needed insight into the observed characteristics while making comparisons with corresponding quasi-steady predictions. Performance of the various configurations is compared on the basis of lift, lift-to-drag ratio, and lift-to-torque ratio.

It has been noted in [5] that it is more difficult to implement mechanical changes in wing kinematics than in wing geometry (i.e., it is easier to install a different-shaped wing than it is to change wing kinematics). Therefore, it is of great interest to study the possibility of achieving favorable aerodynamic characteristics through wing geometry changes. Wing geometry here refers to both its shape and its configuration. This is the theme of this study. The effects on aerodynamic performance of a number of wing geometry parameters are studied using a fixed set of wing kinematics. The parameters in the design space are varied one at a time to identify trends for optimizing wing performance and hence to derive the best

Received 15 November 2007; revision received 11 June 2008; accepted for publication 21 July 2008.

*Research Officer, Department of Aerospace, Power and Sensors. Member AIAA.
†Professor of Aeromechanical Systems, Department of Aerospace, Power and Sensors. Associate Fellow AIAA.
‡Reader in Control Engineering, Department of Aerospace, Power and Sensors. Member AIAA.

combination for a flapping-wing MAV (FMAV). Observations are explained in relation to quasi-steady predictions and the underlying physics of flow. The model used [19,20] is described subsequently, but first, the pertinent aerodynamic phenomena are discussed.

A. Insectlike Flapping

Insect flapping flight has been discussed extensively in [4] and only the features essential to this study are discussed here.

1. *Wing Kinematics*

The description of insect flapping that follows is for two-winged flies (Diptera) from which we draw our inspiration. Insects use a reciprocating wing motion for flight, comparable to the sculling motion of the oars of a rowing boat. This may be decomposed into three component motions: sweeping (fore and aft movement), heaving or plunging (up and down movement), and pitching (varying incidence). Each flapping cycle consists of two half-strokes: a downstroke and an upstroke. These are the translational phases of the flapping cycle because changes in pitch are minimal. At either ends of the half-strokes, the rotational phases of the flapping cycle come into play: stroke reversal occurs, whereby the wing pitches rapidly and reverses direction for the subsequent half-stroke. During this process, the morphological lower surface becomes the upper surface and the leading edge always leads (Fig. 1).

2. *Aerodynamic Phenomena*

The aerodynamics of insect flapping flight is too vast a subject to be addressed in any detail here, and so only the most important flow features germane to hover are described. The flow associated with insect flapping flight is incompressible, laminar, and unsteady and occurs at low Reynolds numbers. The unexpectedly large forces observed can be attributed to a combination of unsteady and vortical aerodynamic effects.

The main identifying feature of an insect's flapping cycle is the wing's start-stop-reversal behavior and this is fundamental to the aerodynamics that make this flight regime possible. The starting vortices shed each time the wing starts are of the opposite sense to the bound circulation and have an inhibitory effect on lift: the so-called *Wagner effect* [22]. Although stroke reversals occur at the end of the half-strokes, there is still significant translational motion during their execution, and the increasing incidence results in an increase in lift: the so-called *Kramer effect* [23]. The converse is true at the start of the subsequent half-stroke when the wing rapidly pitches down.

As a flapping wing moves, it sets the surrounding air in motion. Additional force is required to overcome the repeated acceleration and deceleration of this mass of air: the so-called *apparent mass forces* [24], which must be accounted for. By the very nature of the kinematics, the fluid in the vicinity of the flapping wing is not quiescent (especially during hover or low-speed flight) and *wake capture* forces [25] arise as the wing regularly encounters its own shed wake.

By far, the most important aerodynamic mechanism in insect flight is the *leading-edge vortex* identified by Ellington et al. [26]. They reported that it persisted through each half-stroke and was responsible for the augmented lift forces. They also noted its spanwise-spiraling nature, although this has been questioned by Dickinson et al. [8].

A further feature of insectlike flapping flows is their dependence on the number of semichords traveled [18]. During the development of his model, Ansari [18] noted that when moving spanwise along a flapping wing, a phase difference in vortex-shedding patterns existed between wing sections. Flow in the outboard regions was more developed and older, in terms of semichords traveled, than the inboard regions. More mature flow, having traveled more semichords, was found to be more prone to vortex breakaway. A similar observation was made by Ellington et al. [26], who reported that vortex breakaway caused the leading-edge vortex to lift off the wing surface in the outboard regions of the wing. Wilkins and Knowles [27] also made a similar observation in their computational fluid dynamics (CFD) study on impulsively started rotating wings. Vortex breakaway causes a reduction in lift but an increase in drag. Because outboard wing sections are most likely to be affected, the implications for torque are significant. This behavior is crucial in explaining some of the trends observed in the parametric study presented in Sec. III. The link between flow behavior and flow age in terms of semichords traveled shows that a reduced-frequency-type parameter is still relevant in this form of unsteady flow and stresses the importance of preserving the Strouhal number [27] in experimental investigations, a point also highlighted in [4,20].

Although the model uses 2-D vortex breakaway to explain the variations in the forces observed, in 3-D viscous flow, this is in fact caused by Kelvin–Helmholtz instability in the vortex structures and the merging of the leading-edge vortex with the tip vortex [27]. However, as shown in the following section, the effects of the two mechanisms appear to give corresponding effects, and hence the model of Ansari et al. [19,20] is used in this study.

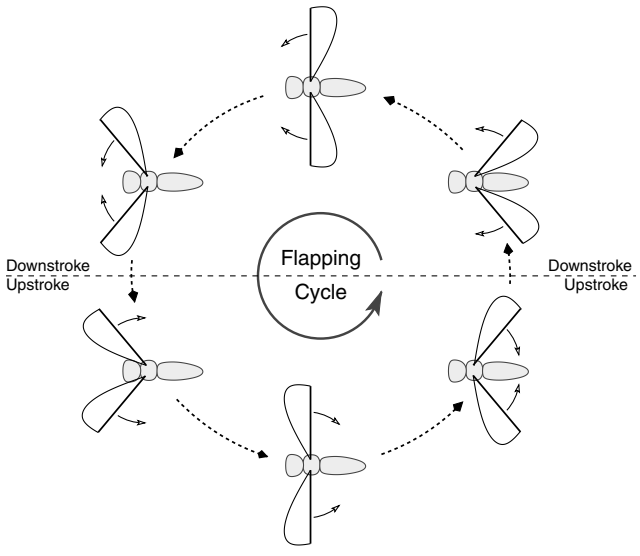

Fig. 1 Half-strokes during insect flapping (bold line marks the wing leading edge).

II. Nonlinear Unsteady Aerodynamic Model

Flapping-wing flows necessitate capturing the separated flow due to the leading-edge vortex and the trailing-edge wake and their complex interaction with the wing (see Fig. 2. Ansari et al. [19,20] developed a nonlinear unsteady aerodynamic model for insect flapping flight in the hover that took into account the flow phenomena mentioned earlier. The model was based on two novel coupled nonlinear integral equations. One of the equations models the leading-edge vortex and the other models the rest of the wake, their coupling expresses the interaction, and the nonlinearity captures wake deformation. The method does not rely on ad hoc adjustments or on empirical fixes (as did many previous models [4]) and shows good agreement with the experiment (see Figs. 2–4). The

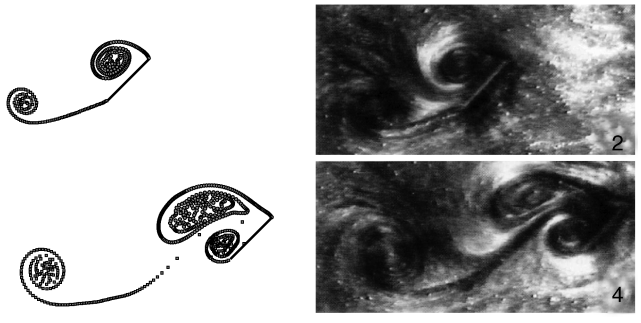

Fig. 2 Theoretical prediction [19,20] of 2-D flow visualization compared with experimental data [31].

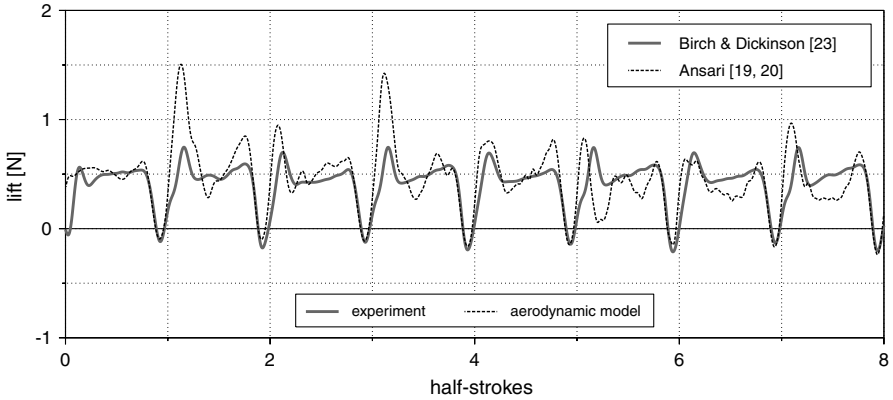

Fig. 3 Theoretical prediction [19,20] of lift force on a 3-D wing compared with experimental data [32].

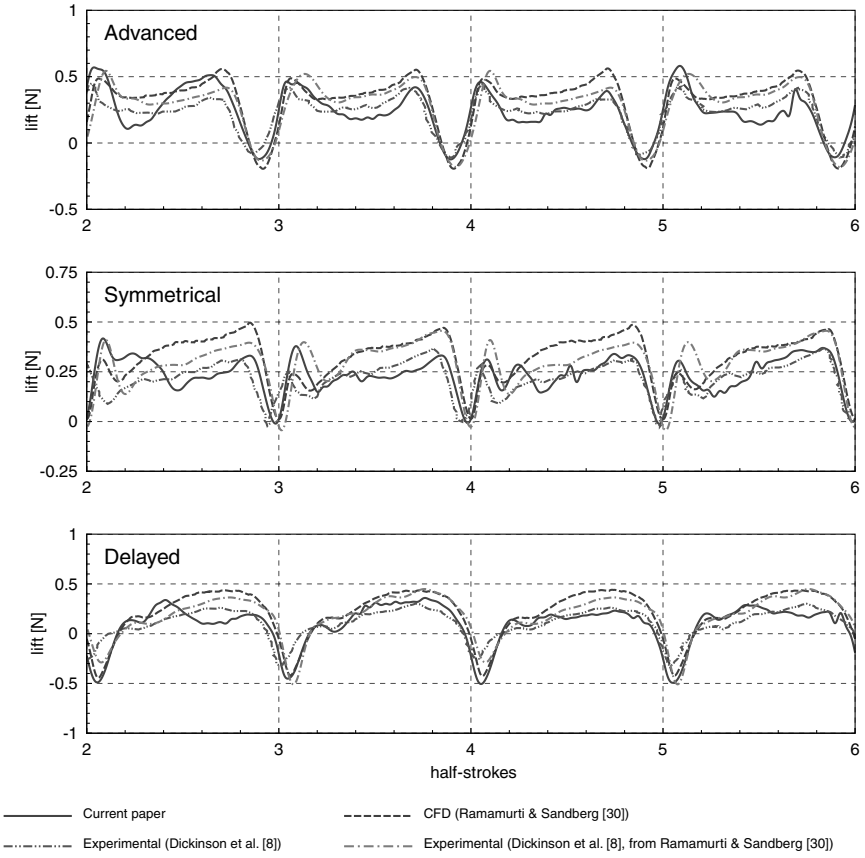

Fig. 4 Plot comparing results from the aerodynamic model used here [19,20] with CFD [28] and experimental measurements [8]. Results shown are for advanced, symmetrical, and delayed kinematics.

interested reader is referred to [19,20] for full details on the model and its accuracy.

With given input kinematics and geometry, the model is capable of returning forces and moments as well as generating flow visualization (see Fig. 5). Producing such a model is challenging, as it necessitates capturing the vortical phenomena and their interaction with the wing, and Ansari et al. [19,20] validated their model for hover (see Figs. 2–4). Figure 4 shows how our aerodynamic model compares with the CFD model of Ramamurti and Sandberg [28]. The wing kinematics for the advanced and delayed cases have a lead and a lag, respectively, of 8% of the flapping cycle on the symmetrical case. Our model produces results

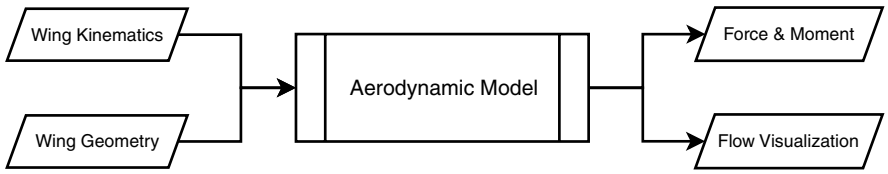

Fig. 5 Data flow in the model of Ansari et al. [19,20].

Table 1 Wing kinematics parameters for all simulations

Parameter	Value
Flapping frequency	2 Hz
Wing motion	Birch and Dickinson [32]
Rotation phase	Advanced by 6% of the flapping cycle (as in [32])

that are consistent with the experimental data of Dickinson et al. [8], whereas the results of Ramamurti and Sandberg [28] compare well with the experimental data of Dickinson et al. [8] that they quote. As highlighted elsewhere [29], more experimental data are needed.

The model of Ansari et al. [20] has been shown to be among the best currently available [4] and was used here for the parametric study. A comprehensive review of other aerodynamic modeling methodologies can be found in [4].

The model [19,20] is quasi-three-dimensional, using a blade-element method to divide the wing spanwise into chordwise strips using radial chords [17,19] that are each treated essentially as two-dimensional. In the current study, the wing section is modeled as a rigid flat plate, but the model is capable of including camber and thickness. Although the insectlike flapping kinematics are spherical, the wings' plunging motion is usually small, and therefore our approach reduces the spherical geometry to a cylindrical one. As a result, each wing section resides in a radial cross plane that is unwrapped flat, and the flow is solved as a planar two-dimensional problem. The overall effect on the wing is obtained by integrating along the span. Because of its quasi-three-dimensional nature, there is no communication between adjacent sections. Hence, spanwise motion of the leading-edge vortex is not treated. The validity of this and the cylindrical-system approximation is discussed in [20]. The impact of neglecting 3-D viscous effects is addressed subsequently.

The aerodynamics were realized using potential flow methods. Because of flow separation from both leading and trailing edges, the Kutta–Joukowski condition is enforced there. The flow is assumed to be irrotational (except at solid boundaries and discontinuities in the wake), and the effects of viscosity are included indirectly in the form of the Kutta–Joukowski condition and in the formation and shedding of vortices. The solution is implemented numerically using a discrete vortex method, and a spin-off of this technique is that flow visualization is generated automatically. Forces and moments are computed by Kelvin's method of impulses [30], and the model was validated against flowfield [31] and force [32] experiments.

The aerodynamic model used here [19,20] does not capture certain 3-D flow features: notably the effects of the tip vortex, spanwise flow, and some aspects of viscosity. These effects will be briefly discussed now.

The effect of the tip vortex on finite wings with attached flow is to reduce lift owing to air spilling from the pressure side of the wing to the suction side. The forward motion of the wing leads to the formation of a trailing vortex system behind the wing, which induces a downwash on the wing. This reduces the effective angle of attack of the wing and thus causes a reduction in lift. By contrast, with suitable wing shaping, the tip vortex can also be used to increase the lift force as in the British Experimental Rotor Program (BERP) helicopter tips [33–35]; this is achieved by managing separated flow over the blade tips. It is therefore difficult to speculate on the net effect of neglecting the tip vortex in our model, in which the flow is predominantly separated.

The spanwise flow in the leading-edge vortex on a flapping wing appears to improve its stability [26,27,36] as vorticity is extracted toward the outboard regions. Because the quasi-3-D model used here does not model this feature, an instability is created that results in vorticity being transported chordwise instead. The leading-edge vortex in each wing section increasingly tends to break away as more chord lengths are swept (a 2-D flow feature [27]). Comparison with experimental data (Figs. 3 and 4), however, shows that the breaking away produces slight oscillations about the measured values of forces, thus giving confidence that the model is correctly capturing total circulation. Indeed, the creation of vorticity in the model is regulated strictly by satisfying the fluid dynamics equations for vorticity balance [19,20].

Aerodynamic modeling progresses from first principles and introduces several simplifications to the basic equations of fluid mechanics, justified by the flow phenomenology and/or geometric and kinematic symmetries [4]. In this way, only some effects of viscosity are included in the current model, such as in the formation of vortices shed into the wake and in the enforcement of the Kutta–Joukowski conditions at the leading and trailing edges. Although vortices shed into the wake are convected in accordance with the Biot–Savart law, their diffusion, which is a feature of viscous flows [37–39], is not implemented in our model. Vortex stretching, which is encountered in 3-D flows [40–42], is also not implemented. The net effect of neglecting diffusion and stretching is difficult to quantify. Vortices that are far removed from the wing are less likely to have much influence, but those in close proximity (as most will be in the hover) may have a greater impact on the flow and hence on forces and moments.

It may be concluded from the preceding discussion that, with the caveats, the model can be used with some confidence as a tool for the study presented here in view of the fact that there is no single clear effect of neglecting these flow features and, more important, because the agreement with experimental data is very encouraging [flow phenomenology, magnitude of the forces, and their unsteadiness are all captured well (see Figs. 2–4)].

III. Wing Geometry Study

The forces and moments experienced by a potential FMAV were obtained by running the simulations for one wing only (the effect of both wings would simply double the quoted values).[§] The fluid medium used was air at standard sea-level atmospheric conditions, and the wing sections were assumed to be rigid flat plates. The required wing kinematics and wing geometry parameters were used as input to the aerodynamic model, and the resulting forces (and related parameters) generated were the outputs used for the comparisons.

Owing to the time-varying nature of the wing forces, performance comparisons are based on mean values of lift $\mathcal{L}$ and drag $\mathcal{D}$, averaged over four half-strokes. Some comparisons are also presented of mean lift-to-torque ratio $\mathcal{L}/\mathcal{Q}$ (indicative of power requirement) and mean lift-to-drag ratio $\mathcal{L}/\mathcal{D}$. When appropriate, plots showing variations in the center of drag (the spanwise radial position at which the resultant drag $\mathcal{D}$ acts) have also been included. These were deduced from the ratio of $\mathcal{L}/\mathcal{D}$ to $\mathcal{L}/\mathcal{Q}$.

Wing kinematics were fixed at the values shown in Table 1, and the effects of varying wing-geometry-related parameters are studied by varying one parameter at a time. The sweep and pitch time histories used were those provided by Birch and Dickinson [32] from their Robofly experiments (e.g., [6]) and are shown in Fig. 6. There is no heave or plunge; hence, the wing tip describes a flat figure eight. The stroke amplitude Φ swept by the Robofly wing was computed as the maximum that was possible without (mechanically) interfering with the other wing (see [5]).

The geometric parameters considered in our investigation were wing aspect ratio, wing length, wing area, wing-offset distance, pitch-axis location, and wing planform shape (see Fig. 7). Pitch-axis location refers to the chordwise position of the spanwise rotational axis of the wing defined along the wing section with the largest chord length. The pitch axis itself is a line drawn radially outward from the center of rotation. Wing-offset distance refers to the distance from the center of rotation to the wing root (Fig. 7). Wing length R is then the distance from the root of the wing to its tip (i.e., length of one wing). The latter is termed the wing-offset distance. Wing area S refers to the planform area of each wing, and aspect ratio $\mathcal{AR}$ is computed from wing length and wing area as $\mathcal{AR} = 4R^2/2S$, in which $\mathcal{AR} =$ (wing span)^2 divided by the total wing area, and the wing span is

[§]In reality, if the wings come in close proximity to one another, some form of mutual interference would come into play, and hence the effect of two wings would not necessarily be the doubling of the single-wing forces.

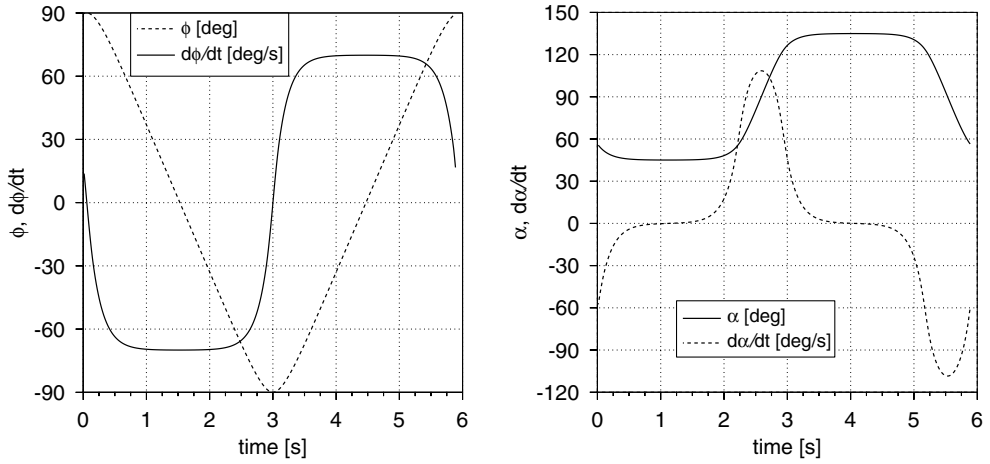

a) Sweep characteristics **b) Pitch characteristics**

Fig. 6 Kinematics of Birch and Dickinson's [32] Robofly showing sweep ($\phi, \dot{\phi}$) and pitch ($\alpha, \dot{\alpha}$) characteristics for one cycle.

twice the length of one wing and so excludes wing offset and any distance between the attachment points of both wings. Note that AR here is based on the total length ($2R$) and total area ($2S$) of both wings and not on the total span (i.e., the effect of offset distance is excluded). Finally, wing planform shape refers to the actual shape of the wing (i.e., rectangular, elliptical, etc.).

Altogether, 13 different planforms were considered (see Fig. 8) and were categorized into two groups. The first group was classified as *symmetric* due to the symmetry of the wings about the spanwise axis through their midchords (Figs. 8a–8f). (Chords are considered here in their usual straight-line sense and not the radial chords shown in Fig. 7.) The second group was *asymmetric* because of the absence of this symmetry about a spanwise axis (Figs. 8g–8m). Each of these wing planforms was investigated for its dependence on the geometry parameters noted earlier, and as these were varied, stroke amplitude changed accordingly. The kinematics provided by Birch and Dickinson (see [32]) were used.

The parameters in the design space are varied one at a time to identify trends for optimizing wing performance and hence finding the best combination for an FMAV. The remaining parameters were maintained at the values shown in Table 2. It may be noted that because wing-offset distance is fixed but aspect ratio AR and wing area S are varied, small changes in stroke amplitude Φ occur because variations in the wing-root chord affect the clearance afforded by the various configurations.

A general trend observed in this study was the similarity between the trends for lift and drag. In the interest of brevity, therefore, only lift plots are shown. The relative effects of drag can be deduced from the lift-to-drag $\mathcal{L}/\mathcal{D}$ and lift-to-torque $\mathcal{L}/\mathcal{Q}$ ratios that are shown.

A. Aspect Ratio

Because lift and drag are functions of wing area S, the effect of aspect ratio AR was investigated by varying wing length R while keeping S constant to enable a fair comparison. All other parameters were maintained at the values shown in Table 2. Figure 9 shows that the trend for the planform shapes considered is that mean lift generally increases with aspect ratio (the results for mean drag are also similar).

From a quasi-steady perspective, doubling aspect ratio would result in doubling lift. Consider, for example, the case of a rectangular wing with length R and mean chord $\bar{c}$. Assuming some mean lift coefficient C_L, the total lift on the wing is

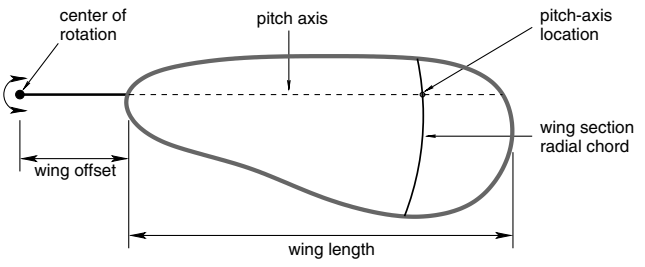

Fig. 7 Wing shape parameters.

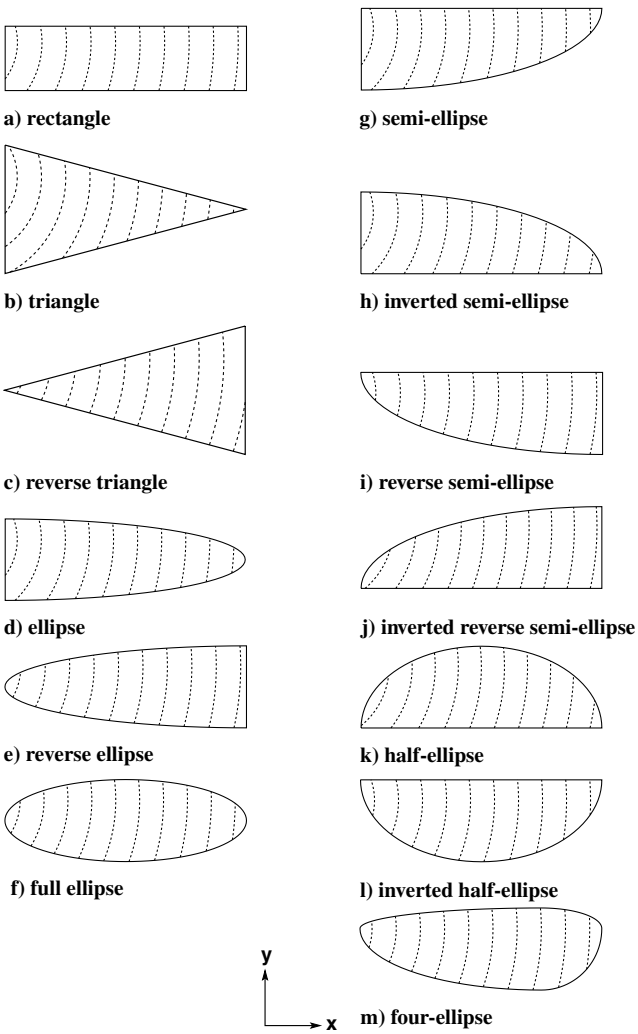

Fig. 8 Symmetric (left) and asymmetric (right) wing planforms (with radial chords shown) used for parametric study. The pitch axis is parallel to the x axis and passes through the center of rotation (which is to the left in each case).

Table 2 Standard wing geometry parameters for simulations

Parameter	Value
Wing length	125 mm
Aspect ratio	7.5
Mean chord	66.67 mm
Pitch-axis location	0.25–chord
Wing area	4167 m^2
Wing offset	25 mm

$$\mathcal{L}_{AR} = \frac{1}{2}\rho C_L \int_0^R (\omega r)^2 \bar{c}\, dr = \frac{1}{2}\rho C_L \omega^2 \bar{c}\frac{R^3}{3}$$

where ρ is air density and ω is sweeping angular velocity. Because aspect ratio is related to wing length and wing chord as $AR \propto R$ and $AR \propto 1/\bar{c}$, respectively,[¶] increasing AR by x means that wing length becomes $\sqrt{x}R$ and wing chord becomes $\bar{c}/\sqrt{x}$.[††] Therefore, lift becomes

$$\mathcal{L}_{xAR} = \frac{1}{2}\rho C_L \omega^2 \frac{\bar{c}\ (\sqrt{x}R)^3}{\sqrt{x}\quad 3} = x\mathcal{L}_{AR}$$

that is, a linear relationship. Some of the plots in Figs. 9a and 9b, however, fall short of this linear relationship. This observation results from the fact that as wing length R increases, mean chord $\bar{c}$ decreases while being exposed to increasing flow velocities (because incident velocity increases radially). This results in the wing getting narrower (in chord length), but traveling more or less the same distance, and so each wing section travels more semichords s as aspect ratio increases. As noted earlier, flow in the outboard sections is more prone to vortex breakaway because of being older in terms of s and hence produces less lift than otherwise expected. Therefore, as aspect ratio increases, the quasi-steady component of lift (in the model of Ansari et al. [19,20], forces and moments can be decomposed into quasi-steady and unsteady components) increases, but is partly countered by the hindering effect of the wake-induced components. [Increasing aspect ratios (narrower wings) allows bigger arcs to be swept. Because the flapping cycles are of the same duration, this increases sweeping angular velocity ω and, from a quasi-steady viewpoint, should increase forces as the square. However, because the forces still increase more or less linearly, the inhibitory effects of the shed wake are made even more obvious.] This results in an increasing deviation from linearity. No apparent differences between the trends for the symmetric and asymmetric planforms can be discerned (cf. Figs. 9a and 9b).

Although the effect of aspect ratio on mean drag is very similar to that observed for mean lift, plots of lift-to-drag ratio $\mathcal{L}/\mathcal{D}$ show an interesting finding (see Fig. 10). For most of the planforms considered, $\mathcal{L}/\mathcal{D}$ reaches a peak for AR in the range of 5–10 and generally does not vary much beyond an aspect ratio $AR \approx 7.5$, implying that there is not much benefit in increasing aspect ratio beyond this value, because drag begins to increase as rapidly as lift. In fact, Ellington [7] noted that aspect ratios found in insects were in the range of 5–12 and that $AR \approx 7$ was a typical value.

The plots for lift-to-torque ratio $\mathcal{L}/\mathcal{Q}$ show diminishing returns for increasing aspect ratio (see Fig. 11). There is a general decline in $\mathcal{L}/\mathcal{Q}$ as aspect ratio increases, implying that more of the outboard region is contributing to the low $\mathcal{L}/\mathcal{D}$; that is, the center of drag[**] is shifting inboard (see Fig. 12), and so it is desirable to keep aspect ratio to a minimum. From a design viewpoint, a compromise would have to be struck between high lift and high $\mathcal{L}/\mathcal{Q}$.

Using a very simplified calculation, Azuma et al. [43] showed that reduced frequency k (which is a measure of flowfield unsteadiness) was related to aspect ratio as $k \propto 1/AR$ for a given stroke amplitude, implying that flapping-wing forces would be expected to more closely approach the quasi-steady limit as AR increased. The present study, however, has shown that the negative effect of sweeping through greater distances s hinders the approach to this quasi-steady limit.

B. Wing Length

The effect of wing length R (with fixed wing area) on the performance characteristics of the flapping wings considered is similar to the description presented earlier for the effect of aspect ratio. The effect on mean lift is shown in Fig. 13. The effect on mean drag is very similar and has been omitted.

There is, however, an important difference between the effects of aspect ratio and wing length on mean lift (cf. Figs. 9 and 13). Whereas the variation of mean lift with aspect ratio was more or less linear, variations in wing length appear to change mean lift more rapidly. In fact, from a quasi-steady analysis, it can be shown that the relationship is quadratic. This can be explained as follows. Using the notation introduced in Sec. III.A, if wing length is increased by x while keeping wing area constant, R becomes xR and mean chord reduces from $\bar{c}$ to $\bar{c}/x$, so that

$$\mathcal{L}_{xR} = \frac{1}{2}\rho C_L \omega^2 \frac{\bar{c}(xR)^3}{x\quad 3} = x^2\mathcal{L}_R$$

In other words, $R \propto AR^2$ so that the plots for variation with wing length explore a wider range of the design space than those for variation with aspect ratio. Deviations from the quadratic predictions arise for the same reasons as were discussed with regard to aspect ratio: outboard regions travel more semichords and are subject to increased vortex breakaway. [The increasing AR associated with increasing R implies that (slightly) longer arcs are swept, further exacerbating this effect.] Hence, mean lift drops and mean drag increases.

The variation in mean lift-to-torque $\mathcal{L}/\mathcal{Q}$ is shown in Fig. 14. Comparing with Fig. 11 shows that the data in Figs. 11 and 14 are complementary (see Fig. 15). From the study on aspect ratio alone, it would appear that $\mathcal{L}/\mathcal{Q}$ increases indefinitely as aspect ratio reduces (Fig. 15), but the study on wing length reveals that the trend in $\mathcal{L}/\mathcal{Q}$, in fact, reaches a peak as aspect ratio gets very small (Fig. 15). This is a valuable insight for wing design. Although the peak in $\mathcal{L}/\mathcal{Q}$ is attractive, it corresponds to a rather small value of lift, and so, in practice, a lower value of $\mathcal{L}/\mathcal{Q}$ and a higher value of lift may make for a more workable design.

C. Wing Area

To investigate the effect of wing area on wing performance, aspect ratio was kept constant so that the shape of the wing planform remained unchanged. The results from this study are shown in Figs. 16–18. Wing area here refers to the planform area of only one of the wings of the wing pair.

The plots for lift and drag are very similar and so only the former are shown. From a quasi-steady perspective, increasing area should be reflected in a linear increase in lift (and drag). In the current flapping-wing case, increases in area are achieved by simultaneous increases in wing length and chord. The variation of lift and drag with wing area would be expected to be quadratic because, for wing area given by $S = R\bar{c}$, then following the notation used in Sec. III.A, if wing area is increased by x, wing length and chord increase as $xS = \sqrt{x}R \cdot \sqrt{x}\bar{c}$. Lift varies linearly with $\bar{c}$ but as the cube of R. Hence, the new lift becomes

$$\mathcal{L}_{xS} = \frac{1}{2}\rho C_L \omega^2 (\sqrt{x}\bar{c})\frac{(\sqrt{x}R)^3}{3} = x^2\mathcal{L}_S$$

The relationship between wing area and lift is found to be slightly less than the quasi-steady predictions. This is not because of vortex breakaway effects (both $\bar{c}$ and R increase with S; hence, the number of semichords traveled is more or less constant), but because larger wings sweep through slightly smaller arcs (because wing offset is fixed) and hence flap slower.

[¶] $AR = 4R^2/2S = 2R^2/\bar{c}R = 2R/\bar{c}$, where, for constant wing area S, the product $\bar{c}R$ must also be constant.

[**] From the definition of torque $\mathcal{Q}$, the radial distance of the center of drag is $(\mathcal{L}/\mathcal{D})/(\mathcal{L}/\mathcal{Q})$.

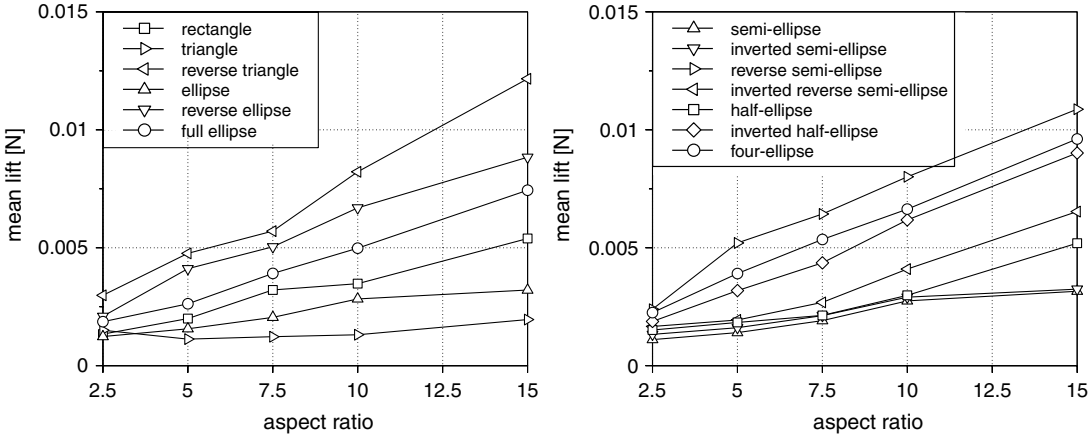

a) Symmetric **b) Asymmetric**

Fig. 9 Effect of aspect ratio on mean lift of symmetric and asymmetric wings.

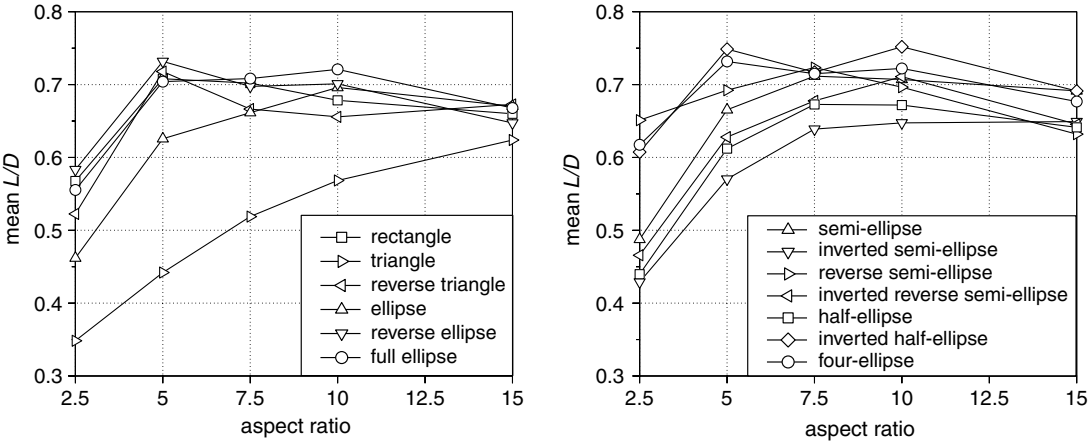

a) Symmetric **b) Asymmetric**

Fig. 10 Effect of aspect ratio on mean lift-to-drag ratio $\mathcal{L}/\mathcal{D}$ of the symmetric and asymmetric wings.

The relationship between mean lift and wing area appears closer to quadratic than was the case for lift vs wing length. This is because wing length R and wing area S are related as $R \propto \sqrt{S}$ (because aspect ratio is constant), and so variations in wing area are achieved by even smaller variations in wing length. In addition, mean chord $\bar{c}$ increases linearly with R, and so the number of semichords traveled s in the outboard regions of the flapping wing does not increase as rapidly as it did for the cases of aspect ratio and wing length considered earlier. Hence, with increases in wing area, vortex breakaway effects are less pronounced and the trend is closer to the parabolic quasi-steady prediction.

In this study, the shape of the wing planforms was preserved (by keeping AR fixed) and only the scale was varied. It would be expected that the lift-to-drag $\mathcal{L}/\mathcal{D}$ characteristics are more or less unaffected

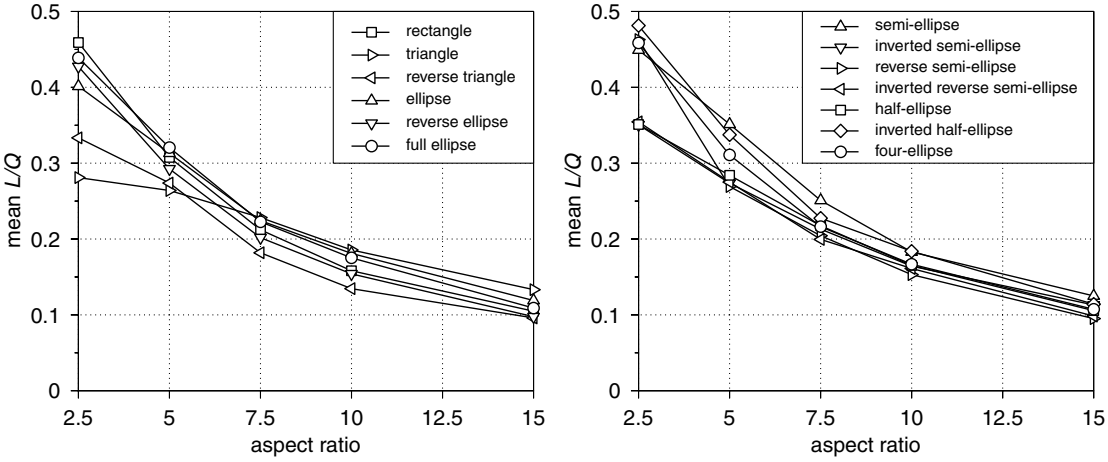

a) Symmetric **b) Asymmetric**

Fig. 11 Effect of aspect ratio on mean lift-to-torque ratio $\mathcal{L}/\mathcal{Q}$ of the symmetric and asymmetric wings.

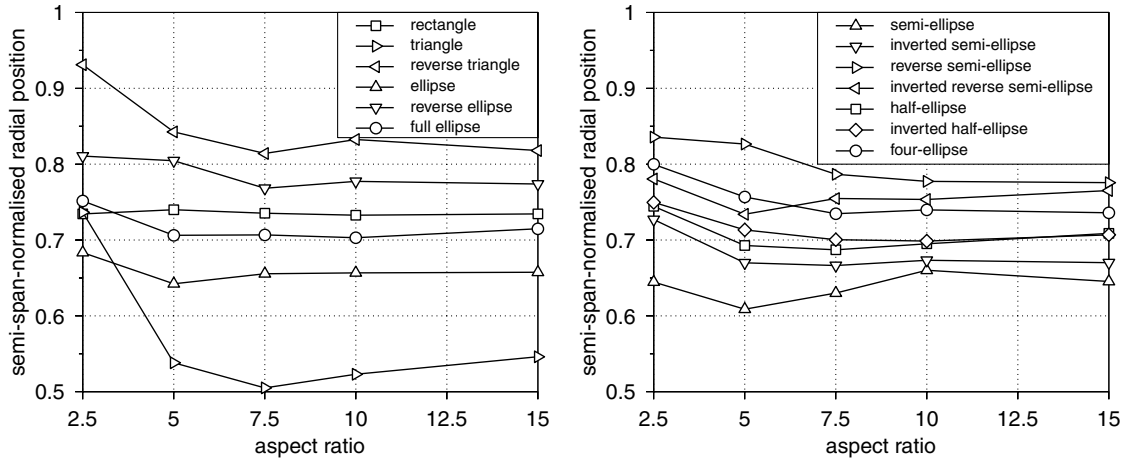

a) Symmetric **b) Asymmetric**

Fig. 12 Effect of aspect ratio on normalized radial position (0 = root, 1 = tip) of the center of drag for the symmetric and asymmetric wings.

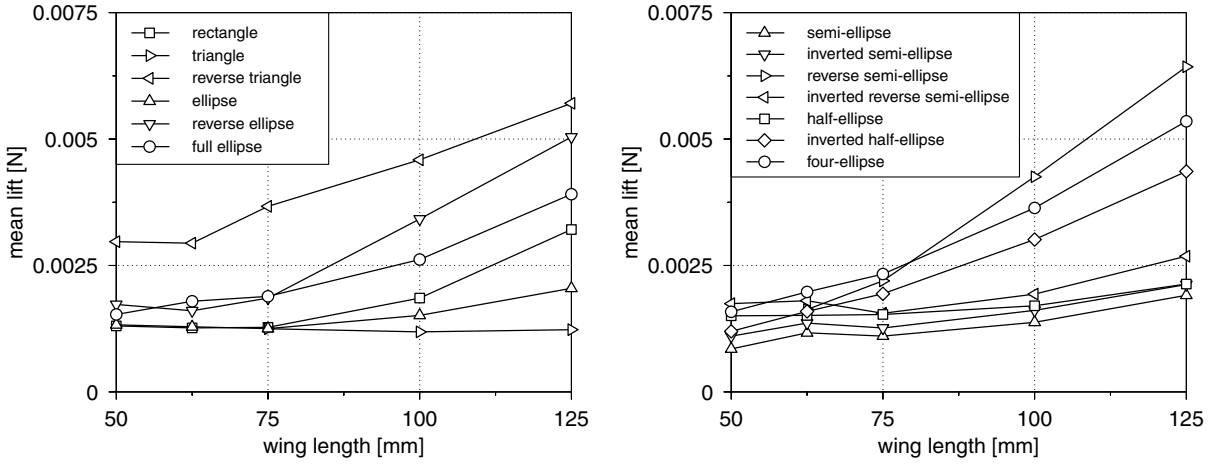

a) Symmetric **b) Asymmetric**

Fig. 13 Effect of wing length on mean lift of the symmetric and asymmetric wings.

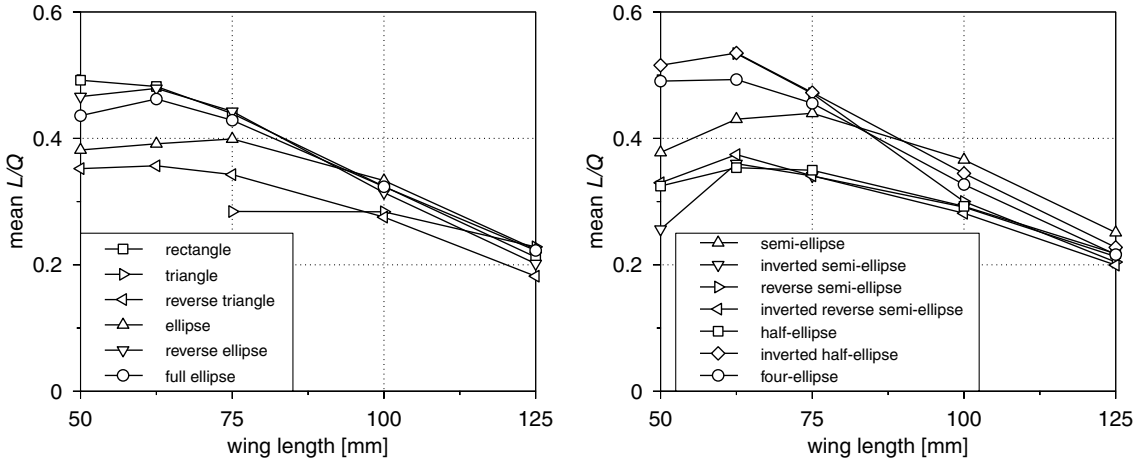

a) Symmetric **b) Asymmetric**

Fig. 14 Effect of wing length on mean lift-to-torque ratio $\mathcal{L}/\mathcal{Q}$ of the symmetric and asymmetric wings.

and this can be seen in Fig. 17. The only deviation is for the triangle planform (Fig. 8b), which shows decreasing $\mathcal{L}/\mathcal{D}$ as S increases. This is mainly because in the outboard regions of the triangle planform, wing chord is much smaller than the other planforms and is therefore the most prone to vortex breakaway and the associated loss of lift and increase in drag. As wing area increases, the wing chord on the inboard side grows significantly (Fig. 8b), whereas wing-offset distance is fixed. As a result, smaller and smaller arcs are swept and lift falls accordingly. At the same time, the radial distance of the outboard regions (where wing chord is small) from the root increases

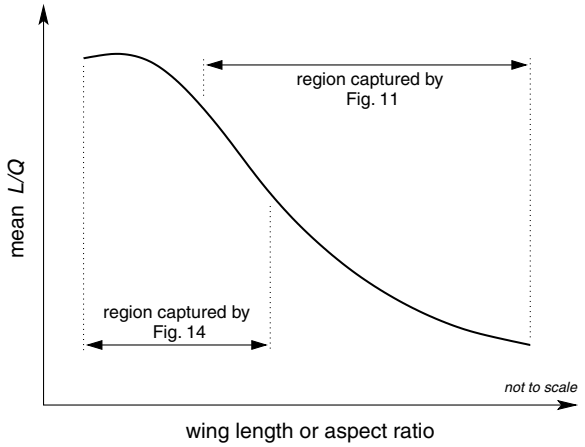

Fig. 15 Range of design space captured by the studies on aspect ratio (Sec. III.A) and wing length (Sec. III.B).

higher lift), because torque would be increasing at the same rate and so would the power requirement for flapping. From a practical viewpoint, there will also be the additional constraints of size, weight, and wing loading. For the asymmetrical wing planforms, this trend appears to be absent for the range of wing areas considered.

D. Wing Offset

The aim of this exercise was to assess the relative merit of increasing wing-offset distance (see Fig. 7) while staying within the 150 mm box for an MAV. Wing-offset distance was varied in the range of 25–75 mm and the wing length was then adjusted accordingly, ensuring that the wing tip did not extend beyond 150 mm from the wing's center of rotation: that is,

$$\text{wing length} = 150\ \text{mm} - \text{wing offset}$$

To enable a fair comparison, wing area was kept constant, and so aspect ratio changed with wing-offset distance, because the wing

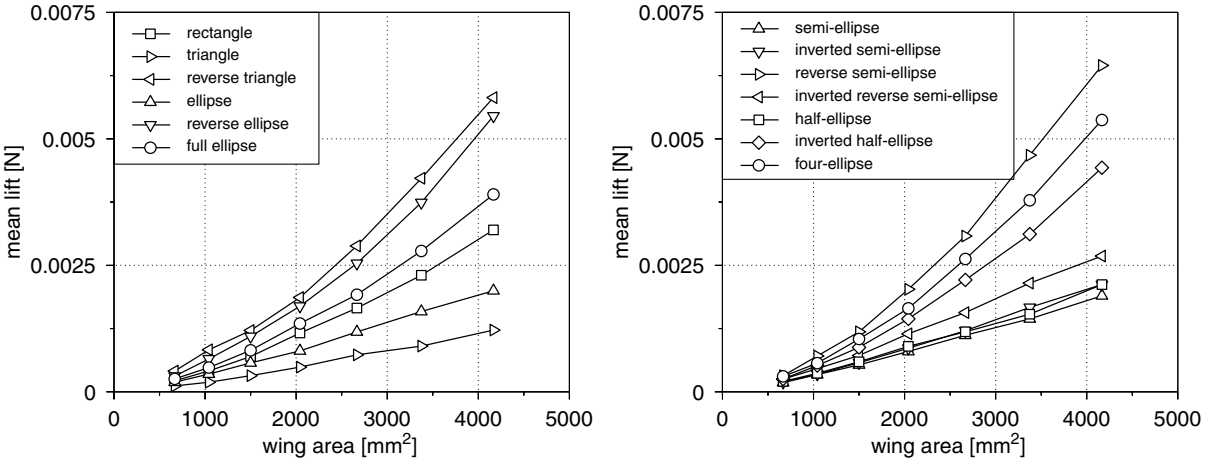

a) Symmetric **b) Asymmetric**

Fig. 16 Effect of wing area on mean lift (for one wing) of the symmetric and asymmetric wings.

and hence and so do the flow velocities there and the distances swept. Greater portions of the wing are exposed to the associated detrimental effects and drag increases rapidly.

The trend in mean lift-to-torque ratio for the symmetrical wing shapes is an initial increase in $\mathcal{L}/\mathcal{Q}$ followed by a plateau that extends from a wing area of about 2000 mm^2 onward (see Fig. 18). The inference to be drawn here is that it is not beneficial to continue increasing wing area beyond a certain point (except for purposes of planform became narrower in chord length as wing-offset distance decreased, and vice versa. The effect of increasing offset distance was to move the wing further away, thus enabling a larger arc to be swept. However, the length of this arc was limited by the corresponding increase in chord length required to keep wing area constant. Figures 19–21 show the main results from this study.

Lift increases almost linearly with increasing wing-offset distance (Fig. 19). The main reason for this effect is that as wing-offset

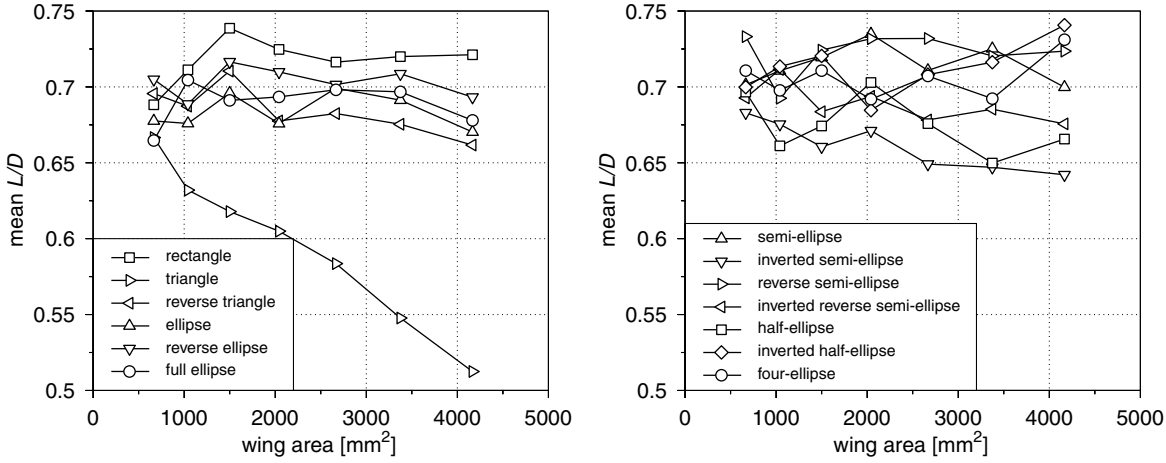

a) Symmetric **b) Asymmetric**

Fig. 17 Effect of wing area on mean lift-to-drag ratio $\mathcal{L}/\mathcal{D}$ of the symmetric and asymmetric wings.

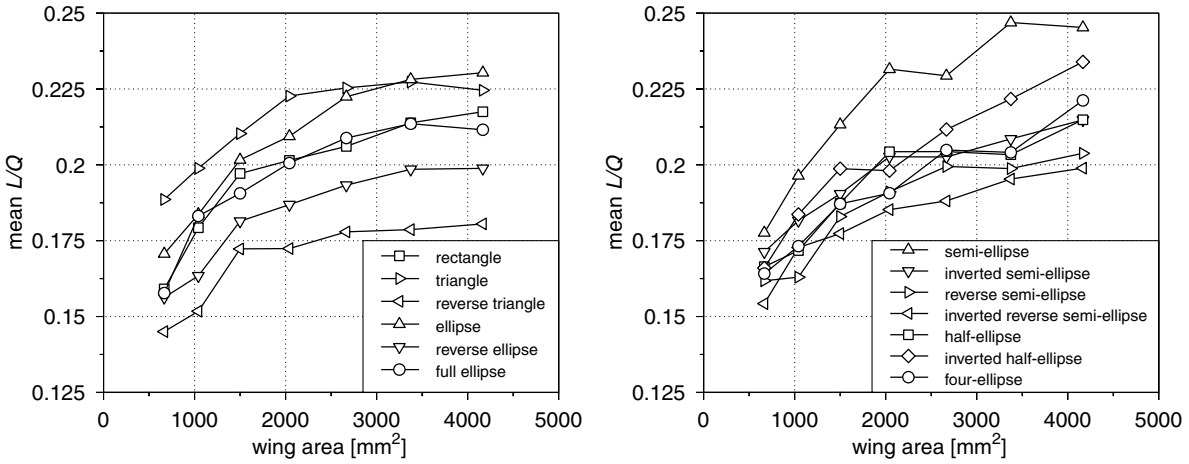

a) Symmetric **b) Asymmetric**

Fig. 18 Effect of wing area on mean lift-to-torque ratio $\mathcal{L}/\mathcal{Q}$ of the symmetric and asymmetric wings.

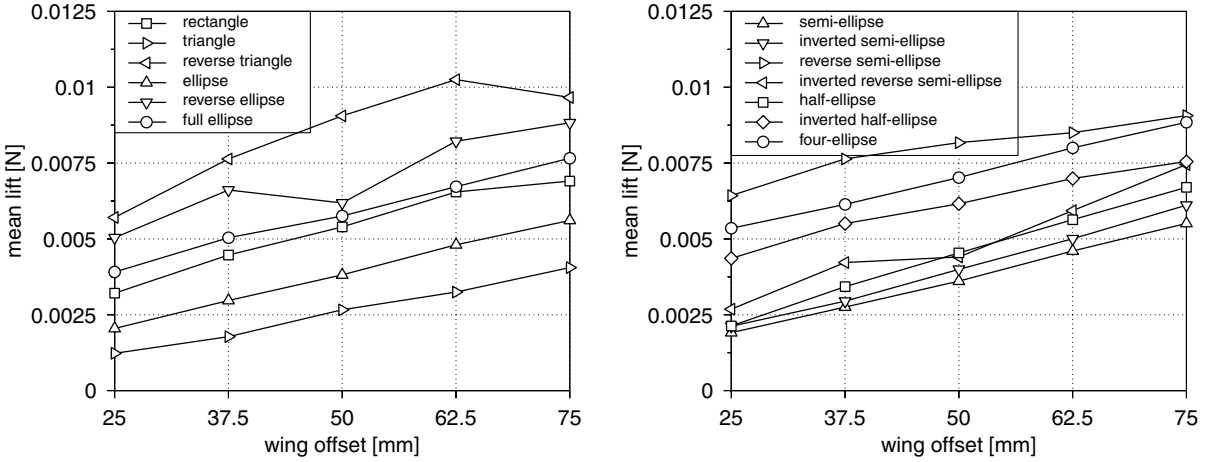

a) Symmetric **b) Asymmetric**

Fig. 19 Effect of wing offset on mean lift of the symmetric and asymmetric wings.

distance increases, more wing area is pushed outboard, where flow velocities are higher. This may be explained by a simple quasi-steady analysis. Assume that the constant wing area to be maintained is S and that mean chord is $\bar{c}$. If wing-offset distance is d and wing extent (radial distance from the center of rotation to the wing tip) is l, then mean chord may be written as $\bar{c} = S/(l-d)$, where wing length $R = l - d$. Then, for a rectangular wing, for example, lift is (see also the analysis in Sec. III.A)

$$\mathcal{L} = \frac{1}{2}\rho C_L \int_d^l (\omega r)^2 \frac{S}{l-d}\mathrm{d}r = \frac{1}{2}\rho C_L \omega^2 S\left(\frac{1}{3}(l-d)^2 + ld\right)$$

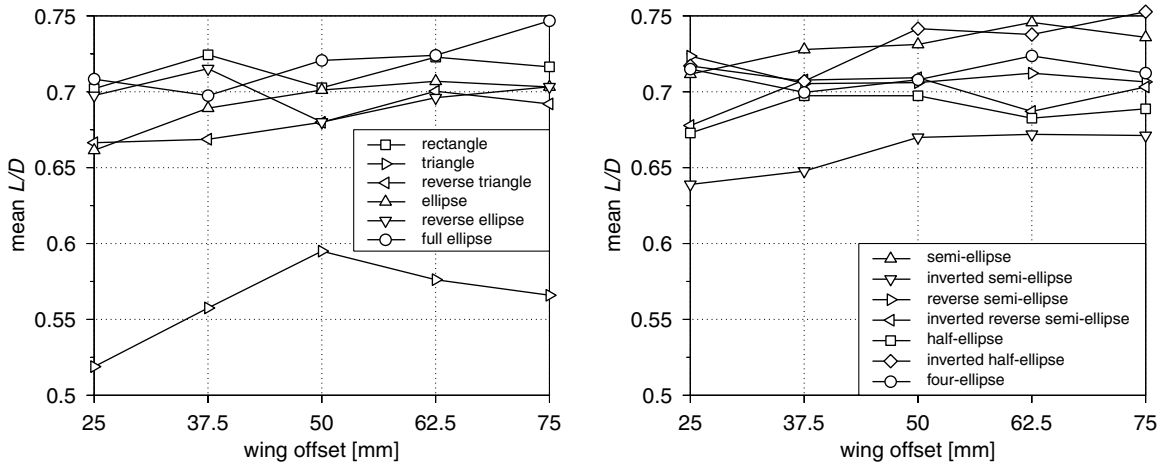

a) Symmetric **b) Asymmetric**

Fig. 20 Effect of wing offset on mean lift-to-drag ratio $\mathcal{L}/\mathcal{D}$ of the symmetric and asymmetric wings.

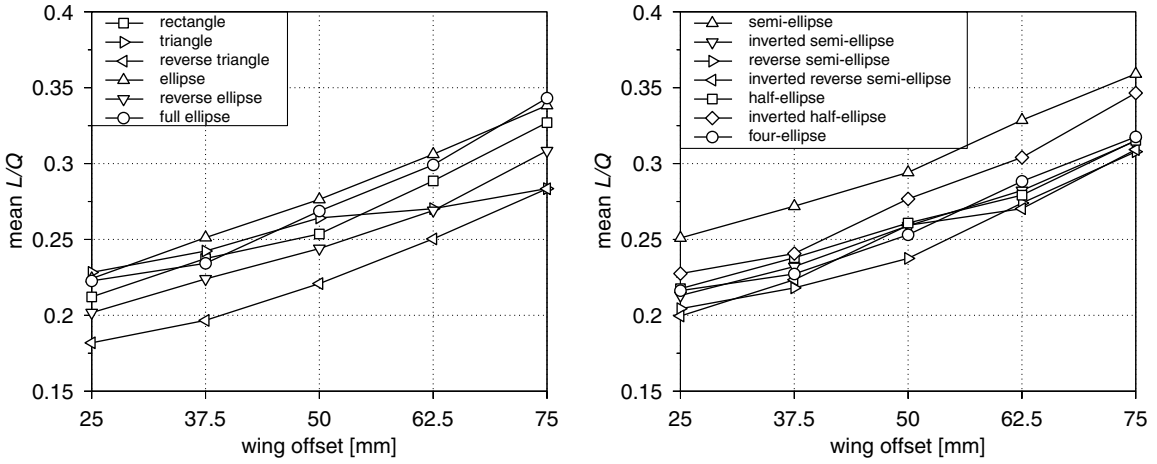

a) Symmetric **b) Asymmetric**

Fig. 21 Effect of wing offset on mean lift-to-torque ratio $\mathcal{L}/\mathcal{Q}$ of the symmetric and asymmetric wings.

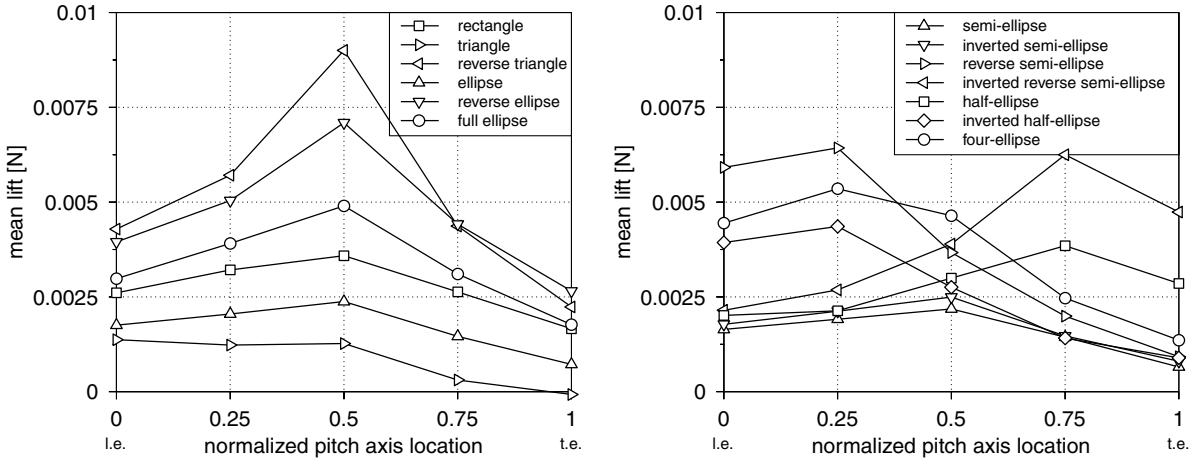

a) Symmetric **b) Asymmetric**

Fig. 22 Effect of pitch-axis location on mean lift of the symmetric and asymmetric wings.

Although the preceding expression is quadratic, its values appear close to linear for the range of d considered here ($1/6 < d/l < 1/2$). The results for drag also show a very similar trend and were omitted.

Whereas increasing wing length resulted in outboard sections becoming increasingly prone to flow breakaway, the effect of increasing wing-offset distance is to make the flow younger in terms of semichords traveled s because mean chord $\bar{c}$ increases with wing-offset distance (wing extent l was limited to 150 mm so that increases in d resulted in smaller R and larger $\bar{c}$ to maintain the same S). Therefore, the flow becomes increasingly stable with growing offset distance. This is manifested in improving lift-to-drag $\mathcal{L}/\mathcal{D}$ and, particularly, lift-to-torque $\mathcal{L}/\mathcal{Q}$ ratios (see Figs. 20 and 21).

Although $\mathcal{L}/\mathcal{D}$ appears to be more or less invariant as wing-offset distance increases (Fig. 20), the $\mathcal{L}/\mathcal{Q}$ plots show a more marked increase for the same range (Fig. 21). The $\mathcal{L}/\mathcal{Q}$ characteristics improve by about 50% for all the wing planforms considered here as wing-offset distance is increased from 25 to 75 mm. It is therefore desirable to have as large a wing offset as possible. However, this will be limited by considerations for low wing-root bending moment and structural stiffness.

E. Pitch-Axis Location

In this study, the position of the spanwise wing rotation (pitching) axis was varied at the location of the maximum chord along the wing (see Fig. 7). For example, for the triangle planform (Fig. 8b), this was measured with respect to the chord length at the wing root, whereas for the reverse triangle (Fig. 8c), it was measured at the wing tip.

For the symmetric wings (Figs. 8a–8f), the pitch-axis location that gave maximum lift was at midchord (see Fig. 22a). For the asymmetric wings (Figs. 8g–8m), this condition was achieved when the wing pitched about the point closest to the chordwise center of area of the planform (see Fig. 22b). A very similar observation was made for the effect on drag.

Consider, for example, the reverse semi-ellipse (Fig. 8i) and the inverted reverse semi-ellipse wings (Fig. 8j). Maximum lift for the former occurred when the pitch axis was located at the quarter-chord point, whereas for the latter (which is its mirror image about a spanwise axis), the same condition was achieved when the wing pitched about the three-quarter-chord point (Fig. 22b). The mean lift plots for wings that are mirror images of each other about some spanwise axis are more or less symmetrical about the midchord points [cf. reverse semi-ellipse and inverted reverse semi-ellipse and also half-ellipse and inverted half-ellipse (see Fig. 22b).][††] The same pattern can be observed for the symmetric wings, on which the mean lift distributions appear more or less symmetric about the midchord point (Fig. 22a).

The location of the pitch axis is significant during the rotational (pitching) phases of the flapping cycle (i.e., at stroke reversals). This

[††]Although the semi-ellipse and inverted semi-ellipse also fall into this category, this trend is less marked in their cases, because both wing shapes have very similar area distributions in inboard regions; see Figs. 8g and 8h, in which most of the forces are generated (this applies to these two planforms specifically; for both wings, the inner 80% of the wingspan generates about 80% of the total force).

is also the phase when peaks and troughs in aerodynamic forces are generated and the relative dominance of these influences the values for mean lift shown in Fig. 22. A similar inference can be drawn for mean drag. To explain these forces, it is necessary to discuss the physics of flow during stroke reversal.

Consider a flapping wing moving from right to left (Fig. 23). As stroke reversal begins (Fig. 23a), the flapping wing rapidly pitches up while slowing down at the same time. The pitch-up and slowdown result in starting and stopping vortices, respectively, being shed from the trailing edge. The relative strength of these determines whether the wing experiences an increase or a decrease in lift. For the purposes of this explanation, we may assume that their net effect is negligible. As stroke reversal proceeds with near-zero translational velocity, a counterclockwise vortex is formed (Fig. 23b) due to the rapid rotation of the wing (referred to as the rotation vortex from here on) and is ejected (Fig. 23c) at a speed dependent on the wing speed at the trailing edge. Immediately thereafter, wing translation begins in the opposite direction and a clockwise starting vortex is also shed (Fig. 23c). Because these two vortices are not collocated, their net effect is not to coalesce, but rather to convect away from the wing (Fig. 23d) at their mutual induced velocities. The effect of the starting vortex is to inhibit the lift on the flapping wing, and so it is beneficial that these vortices convect away as soon as possible. This is made possible if the rotation vortex is ejected at high speed, which in turn requires that the moment arm formed between the center of rotation (the pitch axis) and the trailing edge be as large as possible.

At the leading edge, the situation is somewhat similar. The leading-edge vortex from the previous half-stroke is of the opposite sense to that formed at the start of the new half-stroke and inhibits its growth. Hence, it is desirable to remove it as far as possible from the wing. This again is made possible by shedding it away at the highest possible speed, which is achieved if the moment arm formed by the pitch-axis location and the leading edge is maximized.

Therefore, to maximize lift it is desirable to keep the wing pitch axis as far as possible from both leading and trailing edges. This compromise is achieved best at the midchord position. For the symmetric wing sections, this condition is satisfied by pitching about the midchord position of the wing (hence, the results shown in Fig. 22a). For the asymmetric planform shapes, the midchord position varies along the wing. The best lift is obtained by placing the pitch axis at the midchord position of the wing section with the largest chord length; this corresponds to the locations for maximum lift noted earlier (see Fig. 22b).

The graphs in Fig. 22 show that for the symmetric wings, the same lift and drag can be obtained for two different pitch-axis locations (except for the maximum values) (see Fig. 22a). In a wing-design study, therefore, some other criterion is required to differentiate between pitch-axis locations that give the same lift (and/or drag). This choice can be made by considering the lift-to-torque ratios $\mathcal{L}/\mathcal{Q}$. These are shown in Fig. 24. The results for lift-to-drag ratio $\mathcal{L}/\mathcal{D}$ show the same trends and were omitted.

The trend in mean $\mathcal{L}/\mathcal{Q}$ shows that rearward pitch axes are generally more beneficial. This trend is common to both the symmetric and the asymmetric wings. [Owing to the small magnitudes of the lift and drag generated with wing pitch-axis located at the trailing edge, values of $\mathcal{L}/\mathcal{Q}$ (which involves their ratio) should be treated with caution.] The inference to be drawn here is that it is more important to eject the previous leading-edge vortex than it is to eject the rotation and starting vortices formed at the trailing edge. This is because the latter can convect away at their mutual induced velocities, whereas the previous leading-edge vortex cannot convect far under its own influence.

A comparison of the effect of wing planform shape can also be made here. For the symmetric wings, mean lift at the midchord pitch-axis location shows that the reverse triangle produces the most lift, followed by the reverse ellipse, full ellipse, rectangle, ellipse, and triangle (see Fig. 8). The reason for this is that more lift is produced by wing planforms that have more wing area outboard, where they can make full use of the higher velocities. For the asymmetric wings, the semi-ellipse gives the best lift-to-torque ratio, followed by the inverted half-ellipse, half-ellipse, inverted semi-ellipse, reverse semi-ellipse, and inverted reverse semi-ellipse. The value for the four-ellipse wing occurs somewhere in the middle. The last two wings (reverse semi-ellipse and inverted reverse semi-ellipse) have large chord lengths in the outboard sections. Although this is good from a high-lift perspective, these wing planforms also generate high drag. Hence, they have the lowest $\mathcal{L}/\mathcal{Q}$. Apart from the four-ellipse wing planform, the remaining four planforms have similar chord distributions (see Fig. 8) with near-zero chords in the outboard regions. Most of the lift and drag is generated inboard and these planforms have better $\mathcal{L}/\mathcal{Q}$ characteristics.

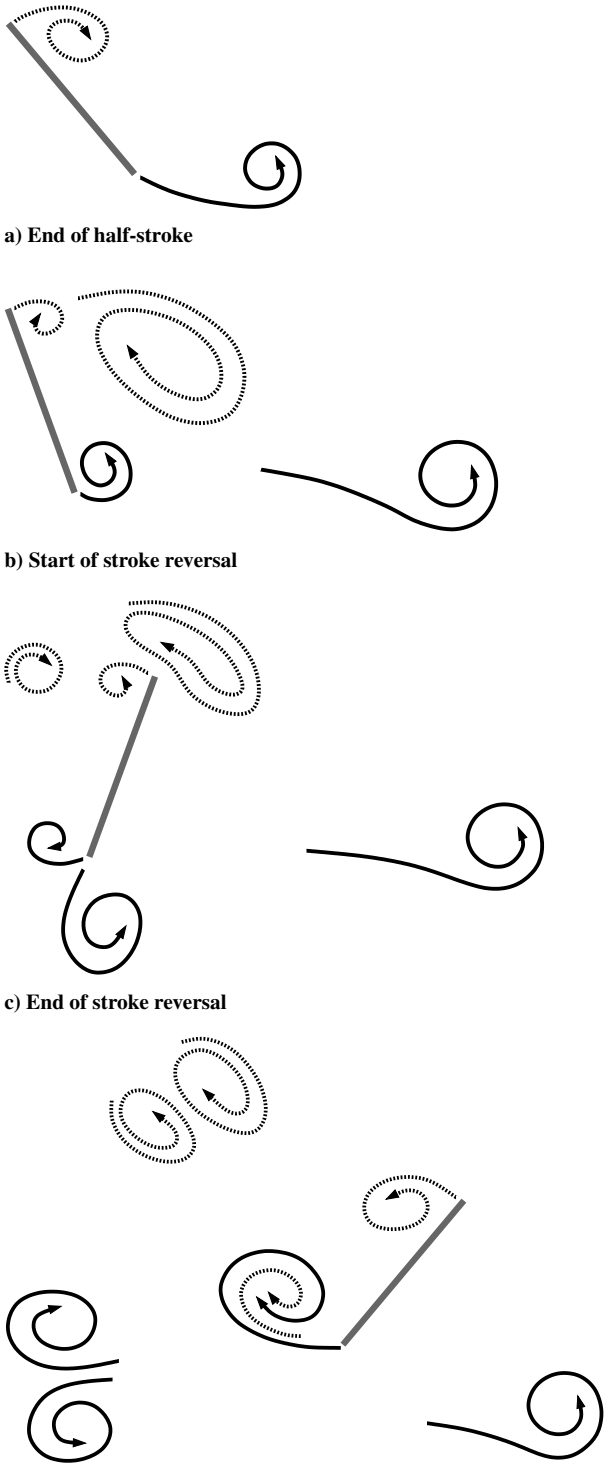

Fig. 23 Typical wake generated by an insectlike flapping wing in the hover (after Ansari [18]). Vortices originating at the leading edge are shown as dotted lines and those from the trailing edge are solid lines.

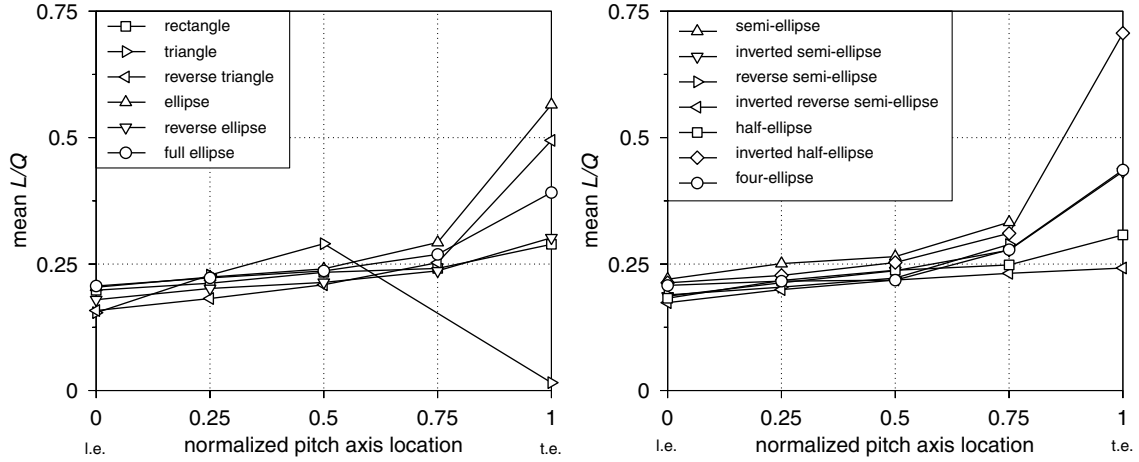

a) Symmetric **b) Asymmetric**

Fig. 24 Effect of pitch-axis location on mean lift-to-torque ratio $\mathcal{L}/\mathcal{Q}$ of the symmetric and asymmetric wings.

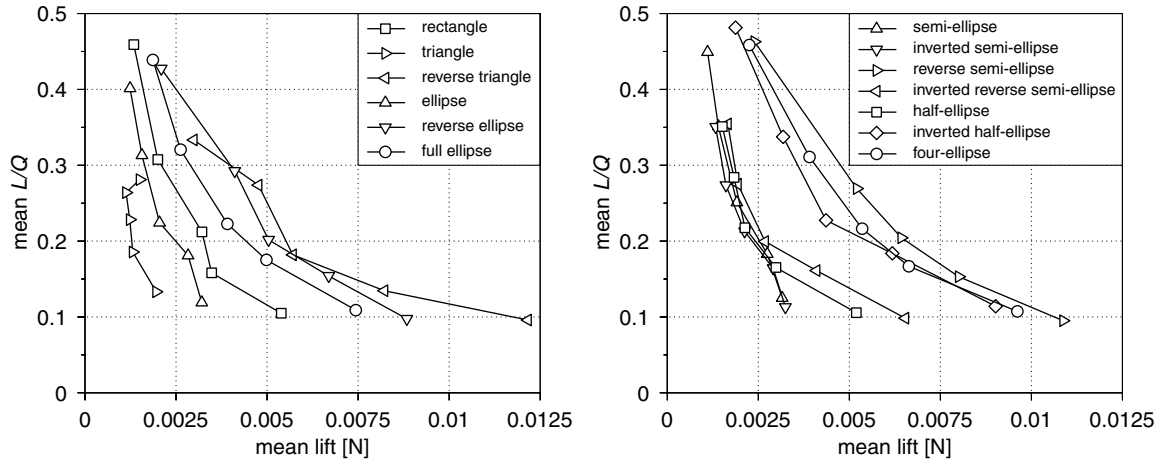

a) Symmetric **b) Asymmetric**

Fig. 25 Mean lift-to-torque ratio $\mathcal{L}/\mathcal{Q}$ vs mean lift as a function of aspect ratio for the symmetric and asymmetric wings.

F. Wing Planform Shape

In this section, the relative merits of all 13 wing planform shapes are discussed. A number of criteria can be used to judge the relative merits. For example, in terms of lift, the following series ranks the wing planforms in order of decreasing lift:

1) The symmetric order is reverse triangle, reverse ellipse, full ellipse, rectangle, ellipse, and triangle.

2) The asymmetric order is reverse semi-ellipse, four-ellipse, inverted half-ellipse, inverted reverse semi-ellipse, half-ellipse, inverted semi-ellipse, and semi-ellipse.

Lift is generally greater for wings with more area outboard, where velocities are higher and hence and so are the forces. From structural considerations, however, it is desirable to keep the wing-root bending moment at a minimum by limiting the level of forces generated outboard so that the preceding order would be in reverse. A compromise would have to be struck between the two opposing requirements for a suitable flapping-wing design.

From a power-requirement perspective, a better measure is lift-to-torque ratio $\mathcal{L}/\mathcal{Q}$. Although a wing with a high $\mathcal{L}/\mathcal{Q}$ is desirable, this wing may not offer a plausible solution if it is unable to generate the desired lift in the first place. For this reason, a plot of $\mathcal{L}/\mathcal{Q}$ against lift is more useful for comparison in wing design. This is shown in Fig. 25 for the range of aspect ratios considered in Sec. III.A. The general trend is that an increase in lift comes at the cost of a reduction in lift-to-torque ratio. Therefore, for maximum power efficiency, it is imperative that lift requirements are kept to a minimum.

Consider, for example, the design requirement for 0.0025 N of lift (the choice of this value has no particular significance from an MAV-design perspective; it was chosen simply because most of the plots in Fig. 25 pass through this point) from a wing planform with minimum torque. This condition is best satisfied by the reverse ellipse from the symmetric wings (Fig. 25a) and by the reverse semi-ellipse from the asymmetric planforms (Fig. 25b). The reverse semi-ellipse wing's $\mathcal{L}/\mathcal{Q}$ value is at least 5% larger than all other wing shapes and at least 15% larger than any of the symmetrical shapes. Figure 25 also shows that wing planforms with straight (or almost straight) leading edges, more wing area outboard, and/or positive sweep at the leading edge show better $\mathcal{L}/\mathcal{Q}$ vs $\mathcal{L}$ characteristics. From a lift-to-torque-ratio perspective, the order of wing planforms with decreasing $\mathcal{L}/\mathcal{Q}$ as a function of $\mathcal{L}$ is more or less the same as for the lift shown earlier. An extra piece of information that can be extracted from Fig. 25 is the range of lift that the wing planforms can offer. The ranking is again the same as that for $\mathcal{L}/\mathcal{Q}$ vs $\mathcal{L}$, implying that a large range of lift depends on there being more area outboard for generating high lift.

IV. Conclusions

In this paper, the influence of wing geometry on the aerodynamic performance of flapping wings in hover was studied for a number of synthetic planform shapes using the aerodynamic model of Ansari et al. [19,20]. The effects of increasing aspect ratio, wing length, and wing area were all to increase lift, albeit at different rates. The effect of increasing wing-offset distance (with fixed overall span) was to improve performance (better lift and lift-to-torque ratios), mainly because more wing area was moved outboard, where flow velocities

are higher. Further, best lift characteristics were extracted when the pitching axis of the wing was located close to the center of the area in the chordwise direction, because it provided the best compromise for ejecting the shed vortices from the leading and trailing edges during stroke reversal. Wing planforms with straight (or almost straight) leading edges and more wing area outboard generally produced better lift and lift-to-torque ratio characteristics.

Most of the studies were compared with quasi-steady predictions, and discrepancies were mainly attributed to the effect of semichords traveled s. Large s was accompanied by a decrease in lift and an increase in drag, giving an overall reduction in aerodynamic performance.

Taking into account the conclusions drawn for the effect of wing kinematics [5], it appears that for an FMAV, the best design configuration would be to flap at a high frequency and sweep through a large stroke amplitude while employing an advanced (early) stroke reversal. In terms of geometry, a configuration that has a considerable wing area outboard while having a high aspect ratio and a straight leading edge would be preferable. In addition, such a configuration would also need to have as large a wing-offset distance as possible and execute pitching rotations about an axis that is close to the wing's center of area in the chordwise direction. As noted in [5], variations in wing geometry are easier to implement than wing kinematics and may therefore be favored in wing design.

The investigation presented here is for insectlike flapping wings *in the hover*. It is possible that the best configuration for other flight regimes (e.g., forward flight) requires a different wing geometry. In practice, the geometry of choice would be determined by the mission profile and may not be optimal for all flight modes. Instead, some kind of weighting may be used for the various flight modes to determine the configuration that gives the best overall performance. Nevertheless, the current study lays useful groundwork for the FMAV flight regime.

Acknowledgments

This work was supported by the Engineering and Physical Sciences Research Council through grants GR/M78472/01 and GR/S23025/01 and by the United Kingdom Ministry of Defence under the Joint Grants Scheme. The authors would also like to thank Michael Dickinson of the California Institute of Technology, Pasadena, CA, for the experimental force data used for validation of the aerodynamic model.

References

[1] Żbikowski, R., "Flapping Wing Autonomous Micro Air Vehicles: Research Programme Outline," *Fourteenth International Conference on Unmanned Air Vehicle Systems*, Bristol Univ., Bristol, England, U.K., 1999, pp. 38.1–38.5.

[2] Żbikowski, R., "Flapping Wing Micro Air Vehicle: A Guided Platform for Microsensors," *Royal Aeronautical Society Conference on Nanotechnology and Microengineering for Future Guided Weapons*, Royal Aeronautical Society, London, 1999, pp. 1.1–1.11.

[3] Żbikowski, R., "Flapping Wing Technology," *European Military Rotorcraft Symposium*, Royal Military College of Science, Shrivenham, England, U.K., 21–23 Mar. 2000, pp. 1–7.

[4] Ansari, S. A., Żbikowski, R., and Knowles, K., "Aerodynamic Modelling of Insectlike Flapping Flight for Micro Air Vehicles," *Progress in Aerospace Sciences*, Vol. 42, No. 2, Feb. 2006, pp. 129–172.
doi:10.1016/j.paerosci.2006.07.001

[5] Ansari, S. A., Knowles, K., and Żbikowski, R., "Insectlike Flapping Wings in the Hover Part 1: Effect of Wing Kinematics," *Journal of Aircraft*, Vol. 45, No. 6, 2008, pp. 1945–1954.
doi:10.2514/1.35311

[6] Ellington, C. P., "The Aerodynamics of Hovering Insect Flight," *Philosophical Transactions of the Royal Society of London, Series B: Biological Sciences*, Vol. 305, Feb. 1984, pp. 1–181.
doi:10.1098/rstb.1984.0049

[7] Ellington, C. P., "The Novel Aerodynamics of Insect Flight: Applications to Micro-Air Vehicles," *Journal of Experimental Biology*, Vol. 202, No. 23, 1999, pp. 3439–3448.

[8] Dickinson, M. H., Lehmann, F. -O., and Sane, S. P., "Wing Rotation and the Aerodynamic Basis of Insect Flight," *Science*, Vol. 284, June 1999, pp. 1954–1960.
doi:10.1126/science.284.5422.1954

[9] Ramamurti, R., and Sandberg, W. C., "A Three-Dimensional Computational Study of the Aerodynamic Mechanisms of Insect Flight," *Journal of Experimental Biology*, Vol. 205, No. 10, 2002, pp. 1507–1518.

[10] Sun, M., and Tang, J., "Lift and Power Requirements of Hovering Flight in Drosophila Virilis," *Journal of Experimental Biology*, Vol. 205, No. 16, 2002, pp. 2413–2427.

[11] Sun, M., and Wu, J. H., "Aerodynamic Forces Generation and Power Requirements in Forward Flight in a Fruit Fly with Modeled Wing Motion," *Journal of Experimental Biology*, Vol. 206, No. 17, 2003, pp. 3065–3083.
doi:10.1242/jeb.00517

[12] Wu, J. H., and Sun, M., "Unsteady Aerodynamic Forces of a Flapping Wing," *Journal of Experimental Biology*, Vol. 207, No. 7, 2004, pp. 1137–1150.
doi:10.1242/jeb.00868

[13] Wu, J., and Sun, M., "The Influence of the Wake of a Flapping Wing on the Production of Aerodynamic Forces," *Acta Mechanica Sinica*, Vol. 21, No. 5, 2005, pp. 411–418.
doi:10.1007/s10409-005-0064-4

[14] Yu, Y., Tong, B., and Ma, H., "An Analytic Approach to Theoretical Modeling of Highly Unsteady Viscous Flow Excited by Wing Flapping in Small Insects," *Acta Mechanica Sinica*, Vol. 19, No. 6, Dec. 2003, pp. 508–516.
doi:10.1007/BF02484543

[15] Yu, Y., and Tong, B., "A Flow Control Mechanism in Wing Flapping with Stroke Asymmetry During Insect Forward Flight," *Acta Mechanica Sinica*, Vol. 21, No. 3, 2005, pp. 218–227.
doi:10.1007/s10409-005-0032-z

[16] Milano, M., and Gharib, M., "Uncovering the Physics of Flapping Flat Plates with Artificial Evolution," *Journal of Fluid Mechanics*, Vol. 534, June 2005, pp. 403–409.
doi:10.1017/S0022112005004842

[17] Ansari, S. A., Knowles, K., and Żbikowski, R., "Aerodynamic Modelling of Some Planforms for Insectlike Flapping Wings," *CEAS Aerospace Aerodynamics Conference*, Royal Aeronautical Society, London, 10–12 June 2003, pp. 38.1–38.14.

[18] Ansari, S. A., "A Nonlinear Unsteady, Aerodynamic Model for Insectlike Flapping Wings in the Hover with Micro Air Vehicle Applications," Ph.D. Thesis, Cranfield Univ., Shrivenham, England, U.K., Sept. 2004.

[19] Ansari, S. A., Żbikowski, R., and Knowles, K., "Non-Linear Unsteady Aerodynamic Model for Insectlike Flapping Wings in the Hover, Part 1: Methodology and Analysis," *Proceedings of the Institution of Mechanical Engineering, Part G: Journal of Aerospace Engineering*, Vol. 220, No. 2, 2006, pp. 61–83.
doi:10.1243/09544100JAERO49

[20] Ansari, S. A., Żbikowski, R., and Knowles, K., "Non-Linear Unsteady Aerodynamic Model for Insectlike Flapping Wings in the Hover, Part 2: Implementation and Validation," *Proceedings of the Institution of Mechanical Engineering, Part G: Journal of Aerospace Engineering*, Vol. 220, No. 3, 2006, pp. 169–186.
doi:10.1243/09544100JAERO50

[21] Ansari, S. A., Knowles, K., and Żbikowski, R., "Design Guidelines for Flapping-Wing Micro UAVs," *SAE 2005 Transactions: Journal of Aerospace*, Mar. 2006, pp. 1–10; also Society of Automotive Engineers Paper 2005-01-3197, 2005.

[22] Wagner, H., "Über die Entstehung des Dynamischen Aufftriebes von Tragflügeln," *Zeitschrift für Angewandte Mathematik und Mechanik*, Vol. 5, No. 1, Feb. 1925, pp. 17–35.
doi:10.1002/zamm.19250050103

[23] Kramer, M., "Die Zunahme des Maximalauftriebes von Tragflügeln bei Plötzlicher Anstellwinkelvergrösserung (Böeneffekt)," *Zeitschrift für Flugtechnik und Motorluftschiffahrt*, Vol. 23, No. 7, Apr. 1932, pp. 185–189; also "Increase in the Maximum Lift of an Airfoil due to a Sudden Increase in its Effective Angle of Attack Resulting from a Gust," NACA TM-678, 1932.

[24] Massey, B., *Mechanics of Fluids*, 7th ed., Stanley Thornes, Cheltenham, England, U.K., 1998.

[25] Dickinson, M. H., "The Effects of Wing Rotation on Unsteady Aerodynamic Performance at Low Reynolds Numbers," *Journal of Experimental Biology*, Vol. 192, No. 1, 1994, pp. 179–206.

[26] Ellington, C. P., van den Berg, C., Willmott, A. P., and Thomas, A. L. R., "Leading-Edge Vortices in Insect Flight," *Nature*, Vol. 384, Dec. 1996, pp. 626–630.
doi:10.1038/384626a0

[27] Wilkins, P., and Knowles, K., "Investigation of Aerodynamics Relevant to Flapping-Wing Micro Air Vehicles," 18th AIAA Computational Fluid Dynamics Conference, AIAA, Reston, VA, June 2007, pp. 1–13; also AIAA Paper 2007-4338, 2007.

[28] Ramamurti, R., and Sandberg, W. C., "Computational Study of 3-D Flapping Foil Flows," 39th AIAA Aerospace Sciences Meeting and Exhibit, AIAA Paper 2001-0605, Reno, NV, Jan. 2001.

[29] Żbikowski, R., Ansari, S. A., and Knowles, K., "On Mathematical Modelling of Insect Flight Dynamics in the Context of Micro Air Vehicles," *Bioinspiration & Biomimetics*, Vol. 1, No. 2, 2006, pp. R26–R37.
doi:10.1088/1748-3182/1/2/R02

[30] Thomson, W. H., "On Vortex Motion," *Transactions of the Royal Society of Edinburgh*, Vol. 25, 1869, pp. 217–260.

[31] Dickinson, M. H., and Götz, K. G., "Unsteady Aerodynamic Performance of Model Wings at Low Reynolds Numbers," *Journal of Experimental Biology*, Vol. 174, No. 1, 1993, pp. 45–64.

[32] Birch, J. M., and Dickinson, M. H., "The Influence of Wing-Wake Interactions on the Production of Aerodynamic Forces in Flapping Flight," *Journal of Experimental Biology*, Vol. 206, No. 13, 2003, pp. 2257–2272.
doi:10.1242/jeb.00381

[33] Brocklehurst, A., and Duque, E. P. N., "Experimental and Numerical Study of the British Experimental Rotor Programme Blade," AIAA 8th Applied Aerodynamics Conference, AIAA Paper 1990-3008, Portland, OR, Aug. 1990.

[34] Duque, E. P. N., "A Numerical Analysis of the British Experimental Rotor Program Blade," *Journal of the American Helicopter Society*, Vol. 37, No. 1, Jan. 1992, pp. 46–54.

[35] Srinivasan, G. R., Raghavan, V., and Duque, E. P. N., "Flowfield Analysis of Modern Helicopter Rotors in Hover by Navier–Stokes Method," *Journal of the American Helicopter Society*, Vol. 38, No. 3, July 1993, pp. 3–13.

[36] Ellington, C. P., "Insects Versus Birds: The Great Divide," 44th AIAA Aerospace Sciences Meeting and Exhibit, AIAA Paper 2006-0035, Reno, NV, Jan. 2006.

[37] Saffman, P. G., *Vortex Dynamics*, Cambridge Monographs on Mechanics and Applied Mathematics, Cambridge Univ. Press, Cambridge, England, U.K., 1992.

[38] Cottet, G. -H., and Koumoutsakos, P. D., *Vortex Methods: Theory and Practice*, Cambridge Univ. Press, Cambridge, England, U.K., 2000.

[39] Majda, A. J., and Bertozzi, A. L., *Vorticity and Incompressible Flow*, Cambridge Texts in Applied Mathematics, Cambridge Univ. Press, Cambridge, England, U.K., 2002.

[40] Ploumhans, P., Winckelmans, G. S., Salmon, J. K., Leonard, A., and Warrene, M. S., "Vortex Methods for Direct Numerical Simulation of Three-Dimensional Bluff Body Flows: Application to the Sphere at $Re = 300$, 500, and 1000," *Journal of Computational Physics*, Vol. 178, No. 2, 2002, pp. 427–463.
doi:10.1006/jcph.2002.7035

[41] Ananthan, S., and Leishman, J. G., "Role of Filament Strain in the Free-Vortex Modeling of Rotor Wakes," *Journal of the American Helicopter Society*, Vol. 49, No. 2, Apr. 2004, pp. 176–191.

[42] Zhao, L., and Tsukamoto, H., "Hybrid Vortex Method for High Reynolds Number Flows Around Three-Dimensional Complex Boundary," *Computers and Fluids*, Vol. 36, No. 7, 2007, pp. 1213–1223.
doi:10.1016/j.compfluid.2007.01.003

[43] Azuma, A., Okamoto, M., and Yasuda, K., "Aerodynamic Characteristics of Wings at Low Reynolds Number," *Fixed and Flapping Wing Aerodynamics for Micro Air Vehicle Applications*, edited by T. J. Mueller, Progress in Astronautics and Aeronautics, Vol. 195, AIAA, Reston, VA, 2001, pp. 341–398.